Mammalian Alkaline Phosphatase Catalysis Requires Active Site Structure Stabilization via the N-Terminal Amino Acid Microenvironment†

Marc F. Hoylaerts,‡,§ Lan Ding,‡ Sonoko Narisawa,‡ Soetkin Van kerckhoven,§ and José Luis Millán*,‡

Burnham Institute for Medical Research, La Jolla, California 92037, and Center for Molecular and Vascular Biology, University of Leuven, Leuven, Belgium

Received December 2, 2005; Revised Manuscript Received June 16, 2006

ABSTRACT: In mammalian alkaline phosphatase (AP) dimers, the N-terminus of one monomer embraces the other, stretching toward its active site. We have analyzed the role of the N-terminus and its microenvironment in determining the enzyme stability and catalysis using human placental (PLAP) and tissue-nonspecific AP (TNAP) as paradigms. Deletion of nine amino acid (aa) residues in PLAP reduced its AP activity and heat stability, while deletion of 25 aa resulted in an inactive enzyme. In turn, deletion of five and nine N-terminal aa in TNAP reduced and abolished AP activity, respectively. The N-terminal aa deletions in both isozymes affected the rate of substrate catalysis (k_{cat}), with an only minor effect on the Michaelis constant (K_m) explained by decelerated intramolecular transition rates in the active site. Arg370 in PLAP, and the corresponding Arg374 in TNAP, critically control the structure and function of the enzymes, but the Glu6−Arg370 bond predicted by the PLAP crystal structure appeared to be irrelevant with respect to PLAP stability or catalysis. Structural disruption was also noted in [R374A]TNAP, [Δ5]TNAP, [Δ9]TNAP, and [Δ25]TNAP using a panel of 19 anti-TNAP antibodies illustrating the structural role of the N-terminus. Our data reveal that the N-terminal α-helical folding is more crucial for the structural stability of the second monomer in TNAP than in PLAP. The correct folding of the N-terminus and of interacting loops in its immediate environment is essential for overall structural integrity and for execution of intramolecular transitions during enzyme catalysis. These findings provide a mechanistic interpretation for loss-of-function mutations of N-terminal TNAP residues in cases of hypophosphatasia.

Alkaline phosphatases (EC 3.1.3.1, APs)[1] are dimeric enzymes present in most, if not all, organisms (*1*). They catalyze the hydrolysis of phosphomonoesters with release of inorganic phosphate. In humans, APs are encoded by four distinct loci. Three isozymes are tissue-specific and 90−98% homologous, i.e., intestinal AP (IAP), placental AP (PLAP), and germ cell AP (GCAP), while the fourth AP isozyme, i.e., tissue-nonspecific (TNAP), is ∼50% identical to the other three isozymes and is expressed in a variety of tissues throughout development (*2*). Our current understanding of the functional properties of mammalian APs comes largely from studies using PLAP and TNAP as paradigms. Isozyme-specific properties, such as the characteristic uncompetitive inhibition properties of mammalian APs (*3*−*5*), their variable heat stability (*6*), and even their allosteric properties (*7*), have been attributed to a top, flexible loop unique to mammalian APs. This domain is also responsible for collagen binding in the case of TNAP (*6*, *8*).

Elucidation of the 1.8 Å resolution structure of human PLAP [PDB entry 1EW2 (*9*)] has facilitated studies of the structure and function of mammalian APs. The overall structure of PLAP is a dimer with each monomer consisting of 484 residues, four metal atoms, one phosphate ion, and 603 water molecules. The two monomers are related by a 2-fold crystallographic axis. The surface of PLAP is poorly conserved compared to that of the *Escherichia coli* enzyme with only 8% of the residues in common. Half of the enzyme surface corresponds to three clearly identifiable regions whose sequences largely vary among human APs and are lacking in nonmammalian enzymes, i.e., a long N-terminal α-helix, an interfacial top flexible loop designated as the "crown domain", and a fourth metal binding domain occupied by calcium (*9*). The availability of the PLAP structure facilitated modeling of the human GCAP, IAP, and TNAP isozymes, revealing that all the novel features discovered in PLAP are conserved in those human isozymes as well (*10*), yet a recently identified structural feature in PLAP, i.e., a peripheral noncatalytic binding site, may confer isozyme-specific properties to this isozyme shared by only some but not other mammalian APs (*11*). An analysis of the structure−function relationship of residues conserved between the *E. coli* AP and the PLAP structure revealed a conserved function for those residues that stabilize the active site Zn

† This work was supported by Grants DE 12889 and AR 47908 from the National Institutes of Health and by the University of Leuven (Geconcerteerde Onderzoeksacties GOA/2004/09).

* To whom correspondence should be addressed: Burnham Institute for Medical Research, La Jolla, CA 92037. Telephone: (858) 646-3130. Fax: (858) 713-6272. E-mail: millan@burnham.org.

‡ Burnham Institute for Medical Research.

§ University of Leuven.

[1] Abbreviations: AP, alkaline phosphatase; GCAP, germ cell alkaline phosphatase; IAP, intestinal alkaline phosphatase; PLAP, placental alkaline phosphatase; TNAP, tissue-nonspecific alkaline phosphatase; FLAG, octapeptide with an Asp-Tyr-Lys-Asp-Asp-Asp-Asp-Lys sequence, used as a tag, recognized by monoclonal anti-FLAG antibody M2; Mes, 2-(*N*-morpholino)ethanesulfonic acid; Mops, 3-(*N*-morpholino)propanesulfonic acid.

10.1021/bi052471+ CCC: $33.50
Published on Web 07/25/2006

and Mg metal ions; the nonhomologous disulfide bonds differ in their structural significance, and nonconserved residues take part in determining the heat stability and uncompetitive inhibition properties of mammalian APs (*12*). In fact, a detailed analysis of PLAP and TNAP mutants has allowed the mapping of the binding site for uncompetitive inhibitors onto the modeled TNAP structure (*13*), and these data will enable drug design efforts aimed at developing improved, specific TNAP inhibitors for therapeutic use given that the genetic and/or pharmacological ablation of TNAP function leads to amelioration of soft-tissue ossification in mouse models of osteoarthritis and ankylosis (*14*, *15*).

Deactivating mutations in the TNAP gene cause the inborn error of metabolism known as hypophosphatasia (*16*), characterized by poorly mineralized cartilage and bones. The severity and expressivity of hypophosphatasia depend on the nature of the TNAP mutation (*17*). The mapping of hypophosphatasia mutations to specific three-dimensional locations on the TNAP molecule has provided clues about the structural significance of these areas for enzyme structure and function (*18*). Mutations have been mapped to all the known important structural motifs of TNAP, including the active site, the crown domain, the calcium site, and the monomer−monomer interface (*18*). Still, some mutations, i.e., Y11C (*19*), A16V (*20*), L20P, A23V, and Q27X (http://www.sesep.uvsq.fr/Database.html), map to the N-terminal arm of TNAP whose precise functional significance has yet to be elucidated. In this paper, we show that the integrity of the N-terminal TNAP arm, in particular the α-helix comprising residues 10−25, and its microenvironment, in particular Arg374, represent structural requirements that the active site needs to adequately execute intramolecular transitions during enzyme catalysis.

EXPERIMENTAL PROCEDURES

Reagents. The QuickChange site-directed mutagenesis kit was purchased from Stratagene (La Jolla, CA); lipofectamine and OPTI-MEM serum free medium were from Invitrogen (Carlsbad, CA). The anti-FLAG monoclonal antibody M2 was from Sigma (St. Louis, MO). The reactivity of a panel of 19 monoclonal antibodies to TNAP has been published (*21*, *22*). Competition studies have organized these antibodies in four only partially overlapping immunological domains on TNAP: A (outer epitopes), B (top domain), C (central domain), and D (C-terminus).

PLAP and TNAP Mutagenesis and Production of FLAG-Tagged Enzymes. Single- and multiple-point mutations and a series of N-terminal deletion mutants were generated in the pcDNA3/PLAP-FLAG vector, using a QuickChange site-directed mutagenesis kit as described previously (*12*). Oligonucleotides used in this study are listed in Table 1. PCR products and constructs were sequenced to verify the correct introduction of mutations into the sequence. PLAP−FLAG and TNAP−FLAG constructs, in which the FLAG sequence is substituted for the GPI anchor, were then transiently transfected into COS-1 cells with lipofectamine 2000 reagent. Transfected cells were cultured in OPTI-MEM serum-free medium, and conditioned media [containing secreted wild-type (wt) and mutant enzymes] were collected 48 h after transfection.

AP Assays and Kinetic Measurements. All kinetic measurements were performed in triplicate at 25 °C. For the measurement of relative catalytic activities, microtiter plates were coated with the M2 antibody (depending on the experiment, ranging from 0.2 to 1 μg/mL). For the calculation of catalytic rate constants (k_{cat}), we used the PLAP−FLAG construct with a known k_{cat} (460 s^{-1}) as a reference for each microtiter plate (*5*). Recombinant APs were incubated with the plates for 2 h at room temperature, after which plates were washed with PBS, containing 0.008% Tween 80. The AP activity of bound enzymes or enzyme mutants was then measured at 405 nm as a function of time, using *p*-nitrophenyl phosphate (pNPP, 0.05−20 mM) as a substrate, either at pH 9.8 in 1 M diethanolamine buffer containing 1 mM $MgCl_2$ and 20 μM $ZnCl_2$ or at pH 7.5 in 1 M Tris-HCl containing 1 mM $MgCl_2$ and 20 μM $ZnCl_2$, as indicated. Recordings for kinetic computation were selected from those parts of the curve where *A*(405 nm) versus time was linear, and reaction rates were recorded as Δ*A*(405 nm) per minute, taking into account an extinction coefficient for reaction product *p*-nitrophenol of 12.2×10^3 M^{-1} cm^{-1}, when measured at pH 9.8 in 1 M diethanolamine buffer containing 1 mM $MgCl_2$ and 20 μM $ZnCl_2$, or 10.3×10^3 M^{-1} cm^{-1}, when measured at pH 7.5 in 1 M Tris-HCl containing 1 mM $MgCl_2$ and 20 μM $ZnCl_2$. Thus, initial rates were calculated over a time interval of up to 2 h, excluding the first 5 min from evaluation, because of non-steady-state conditions. Data were linearized in $1/v$ versus substrate Michaelis−Menten concentration plots, and linear regression was performed, calculating slopes ± the standard deviation (SD) and intercepts ± SD in GraphPad Prism version 3.0a (GraphPad Software, San Diego, CA).

To measure the heat stability of PLAP and its mutants, enzymes were incubated at 65 °C in 1 M diethanolamine (pH 9.8) containing 1 mM $MgCl_2$ and 20 μM $ZnCl_2$. Samples were removed at different time points and placed in ice and residual activity was then measured as explained above, with 20 mM pNPP. Likewise, the heat stability of TNAP and its mutants was measured in the same buffer, at 56 °C, as a function of time.

Inhibition studies in the presence of competitive AP inhibitor Na_3PO_4 (0−50 mM) and uncompetitive inhibitors L-Phe (0−40 mM) and L-homoArg (0−40 mM) were carried out essentially in the same manner, at both pH 7.5 and 9.8, as explained above. In addition, double-reciprocal plots were constructed for the inhibition at pH 7.5 of PLAP by L-Phe (0−20 mM) and of TNAP by L-homoArg (0−80 mM), upon assessment of pNPP (0.2−2 mM) hydrolysis for each inhibitor concentration.

The effect of viscosity modulation on PLAP and TNAP activity was measured in 0.04 M Mes buffer (pH 6.0), in 0.04 M Mops buffer (pH 8.0) (23), in 1 M Tris-HCl buffer (pH 7.5), and in 1 M DEA buffer (pH 9.8), all buffers containing 1 mM $MgCl_2$ and 20 μM $ZnCl_2$, in the presence of increasing concentrations of sucrose (0−35% weight to volume) (*23*, *24*). The impact of transphosphorylation during catalysis by PLAP and TNAP was measured by variation of the diethanolamine concentration (from 0 to 1 M), at pH 9.8.

Conformational Analysis of TNAP Mutants. To analyze the impact of N-terminal deletions on the overall TNAP structure, the ISOBM TD-9 Workshop antibody panel of epitope-mapped monoclonal anti-TNAP antibodies (*21*, *22*) was coated onto microtiter plates at 5 μg/mL, overnight at

Table 1: Identification of pcDNA3/PLAP−FLAG and pcDNA3/TNAP−FLAG Constructs[a]

name	PCR primers (5′−3′) region encoded
	Placental Alkaline Phosphatase (PLAP)
[Δ1]PLAP	CAGCTCTCCCTGGGCATCCCAGTTGAGGAG full-length PLAP lacking residue 1
[Δ2] PLAP	GCTCTCCCTGGGCCCAGTTGAGGAGG full-length PLAP lacking residues 1 and 2
[Δ3]PLAP	GCTCTCCCTGGGCGTTGAGGAGGAG full-length PLAP lacking residues 1−3
[Δ5]PLAP	GCTCTCCCTGGGCGAGGAGAACCCG full-length PLAP lacking residues 1−5
[Δ7]PLAP	GCTCTCCCTGGGCAACCCGGACTTC full-length PLAP lacking residues 1−7
[Δ9]PLAP	CAGCTCTCCCTGGGCGACTTCTGGAACCGC full-length PLAP lacking residues 1−9
[Δ25]PLAP	CAGCTCTCCCTGGGCCTGCAGCCTGCACAGACA full-length PLAP lacking residues 1−25
[E7K]PLAP	CATCCCAGTTGAGGAGAAGAACCCGGACTTC full-length PLAP with the E7K mutation
[R370A]PLAP	CCTTCGGAGGCTACCCCCTGGCAGGGAGCTCCATCTTCGGGC full-length PLAP with the R370A mutation
	Tissue-Nonspecific Alkaline Phosphatase (TNAP)
[Δ1]TNAP	CCTGCCTTACTAACTCCGTGCCAGAGAAAGAG full-length TNAP lacking residue 1
[Δ2]TNAP	CCTGCCTTACTAACTCCCCAGAGAAAGAGAAAG full-length TNAP lacking residues 1 and 2
[Δ3]TNAP	CTGCCTTACTAACTCCGAGAAAGAGAAAGAC full-length TNAP lacking residues 1−3
[Δ5]TNAP	CCTGCCTTACTAACTCCGAGAAAGACCCCAAG full-length TNAP lacking residues 1−5
[Δ9]TNAP	CTGCCTTACTAACTCCAAGTACTGGCGAGACC full-length TNAP lacking residues 1−9
[Δ25]TNAP	CTGCCTTACTAACTCCCTTCAGAAGCTCAACACC full-length TNAP lacking residues 1−25
[K7E]TNAP	GTGCCAGAGAAAGAGGAGGACCCCAAGTACTGGC full-length TNAP with the K7E mutation
[Y371A]TNAP	CTTCACATTTGGTGGAGCCACCCCCCGTGGCAACTCT full-length TNAP with the Y371A mutation
[R374A]TNAP	CATTTGGTGGATACACCCCCGCTGGCAACTCTATCTTTGGTC full-length TNAP with the R374A mutation

[a] The nomenclature of various recombinant PLAP and TNAP proteins and PCR primers used to generate mutants is shown. Primers are forward primers.

4 °C. After the samples had been blocked with 1% bovine serum albumin in PBS, containing 0.008% Tween 80 for 30 min, saturating concentrations of TNAP, [Δ5]TNAP, [Δ9]TNAP, [Δ25]TNAP, [R374A]TNAP, and [Y371A]TNAP were incubated in the plates for 2 h at room temperature. After being washed, the bound enzyme was detected with biotinylated M2 antibody and avidin−biotin peroxidase, according to standard ELISA procedures. To exclude the possibility that some of the antibodies would recognize linear epitopes on TNAP N-terminal sequences, binding of TNAP to these antibodies was also tested in the presence of synthesized peptides LVPEKEKDP (9-mer, 0−100 μM) and LVPEKEKDPKYWRDQ (15-mer, 0−200 μM), corresponding to the TNAP N-terminal sequence.

α-Helical Propensity Calculation in TNAP and Its N-Terminal Deletion Mutant. To estimate whether deletion of nine N-terminal amino acid (aa) residues would affect the α-helical folding of the TNAP structure, peptide folding in solution was assessed, using the Pepstr server, choosing a hydrophobic peptide environment (www.imtech.res.in/raghava/pepstr/home.html). The Pepstr server predicts the tertiary structure of small peptides with 7−25 residues, on the basis of the assumption that β-turns are an important and consistent feature of small peptides. The methods use regular secondary structure information predicted from PSIPRED and β-turn information predicted from BetaTurns. Side chain angles were placed using standard the backbone-dependent rotamer library, and structures were further refined with energy minimization and molecular dynamic simulations using Amber version 6.

Mechanism of Catalysis. The kinetic data in this study were analyzed according to the classical mechanism of *E. coli* AP enzyme catalysis, outlined in Scheme 1. In this

Scheme 1

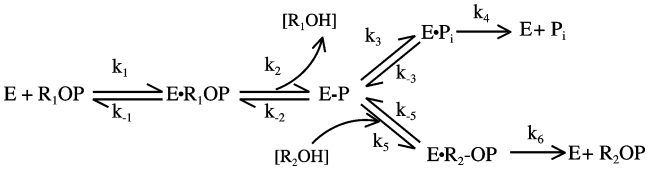

general model of AP catalysis, substrate positioning in the active site is controlled via forward and reverse rate constants k_1 and k_{-1}, respectively, whereas intramolecular covalent phospho-complex formation in the active site (E−P) is described by rate constants k_2 and k_{-2}. Enzyme regeneration requires hydrolytic product formation (E−P to E•P_i, de-

Table 2: Relative First-Order Enzyme Activity [ΔA(405 nm) per minute][a] as a Function of pH and Buffer Composition, Viscosity, and Transphosphorylation

sucrose (%, w/v)	0.04 M Mes (pH 6.0)		0.04 M Mops (pH 8.0)		1 M Tris-HCl (pH 7.5)		1 M DEA (pH 9.8)[b]	
	PLAP	TNAP	PLAP	TNAP	PLAP	TNAP	PLAP	TNAP
0	0.33	0.26	1.78	0.77	2.6	0.58	18.3	9.2
5	0.39	0.33	1.78	0.87	2.5	0.56	16.6	8.6
10	0.45	0.35	1.76	0.93	2.5	0.56	15.4	7.7
15	0.27	0.38	1.89	0.98	2.5	0.51	13.9	7.1
20	0.30	0.36	1.85	0.81	2.0	0.44	12.8	6.0
25	0.34	0.25	1.53	0.74	1.7	0.36	10.8	5.3
30	0.31	0.26	1.37	0.65	1.6	0.34	8.8	4.4
35	0.32	0.29	1.49	0.75	1.3	0.33	7.7	3.6

	pH 9.8[c]	
[DEA] (M)	PLAP	TNAP
0.063	0.077	0.072
0.125	0.97	0.5
0.25	3.9	1.1
0.5	8.3	2.5
1	13. 7	4.0

[a] Activity was measured every minute over an interval of 1 h, and slopes were calculated from the best fit over this time interval; they were corrected for spontaneous pNPP hydrolysis in the corresponding buffer, during the same time interval. All buffers contain 20 μM $ZnCl_2$ and 2 mM $MgCl_2$ and a saturating pNPP concentration of 20 mM. [b] Enzyme activity is measured as a function of sucrose concentration, in 1 M DEA. [c] Enzyme function is measured as a function of DEA concentration, in the absence of sucrose. In comparison to the enzyme concentration tested in 1 M DEA buffer (pH 9.8), PLAP and TNAP are 5-fold more concentrated in 1 M Tris-HCl buffer (pH 7.5), 25-fold more concentrated in 0.04 M Mops buffer (pH 8), and even 2500-fold more concentrated in 0.04 M Mes buffer (pH 6).

scribed by rate constants k_3 and k_{-3}) and subsequent product release (dissociation of E·P_i into E and free phosphate, described by k_4). In nucleophilic buffers (presence of R_2OH), catalysis at high pH is dramatically enhanced via transphosphorylation-assisted hydrolysis, described by k_5 and k_{-5}, the resulting phosphate esters rapidly dissociating (described by k_6) from the enzyme,

It is reported for *E. coli* AP (*24*) that the catalytic rate constant is limited by product release at pH >8 and by hydrolysis of the phosphoserine intermediate at pH <6. We herein also confirm that PLAP and TNAP catalysis could be affected by viscosity (see Table 2). Moreover, 1 M DEA strongly stimulates catalysis, as a consequence of transphosphorylation (see Table 2). In addition, tris(hydroxymethyl)-aminomethane is also a good phophoryl acceptor and causes a large increase in the maximal velocity, because Tris phosphate dissociates rapidly, bypassing the slow dissociation of inorganic phosphate from the enzyme (*25*) (see Table 2). Because essentially all our enzyme mutant analyses are carried out in the presence of 1 M DEA or 1 M Tris, we can therefore simplify the general reaction scheme as shown in Scheme 2. In Scheme 2, valid at pH 7.5 and 9.8, the rate-

Scheme 2

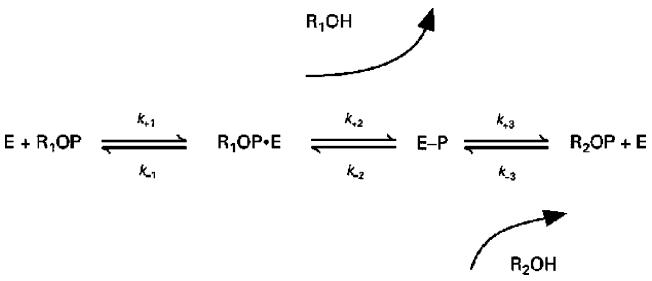

limiting hydrolysis of the phosphoserine complex is eliminated and k_3 and k_{-3} (*5*) now represent rate constants combining transphosphorylation and non-rate-limiting dissociation of R_2OP. This model is therefore characterized by the following expressions for K_m and k_{cat}, respectively.

$$k_{cat} = \frac{k_2}{1 + k_2/k_3}$$

$$K_m = \frac{k_{-1} + k_2}{k_1(1 + k_2/k_3)}$$

$$k_{cat}/K_m = \frac{k_1}{1 + k_{-1}/k_2}$$

$$K_{EPI} = \frac{[E{-}P][I]^\circ}{[E{-}P{\cdot}I]} \quad (1)$$

where $K_i = K_{EPI}(1 + k_3/k_2)$. Inhibition by uncompetitive inhibitors, i.e., inhibitors (I), acting at the level of the E−P intermediate, is described by a K_i value, which depends on equilibrium constant K_{EPI} and on the rate of phosphorylation and dephosphorylation (*5*). Because K_i contains rate constant k_3, its numerical value depends on pH and buffer composition. In view of the inhibitor protonation, K_{EPI} also depends on pH.

RESULTS

Structural Determinants of PLAP N-Terminal Sequences. On the basis of the human PLAP crystal structure (*9*), Figure 1a illustrates how the 25 N-terminal aa residues of PLAP monomer A extend over monomer B. The first nine aa residues point toward a loop in monomer A, important for enzyme catalysis, since it harbors residue Y367 that points toward the active site of monomer B (*12*). Figure 1b identifies two residues in this nine-aa sequence that are capable of structural stabilization through side chain interactions, i.e., Glu6 (monomer A) with Arg370 (monomer A), separated by 2.86 Å (nr 1), and Glu7 (monomer A) with Arg117

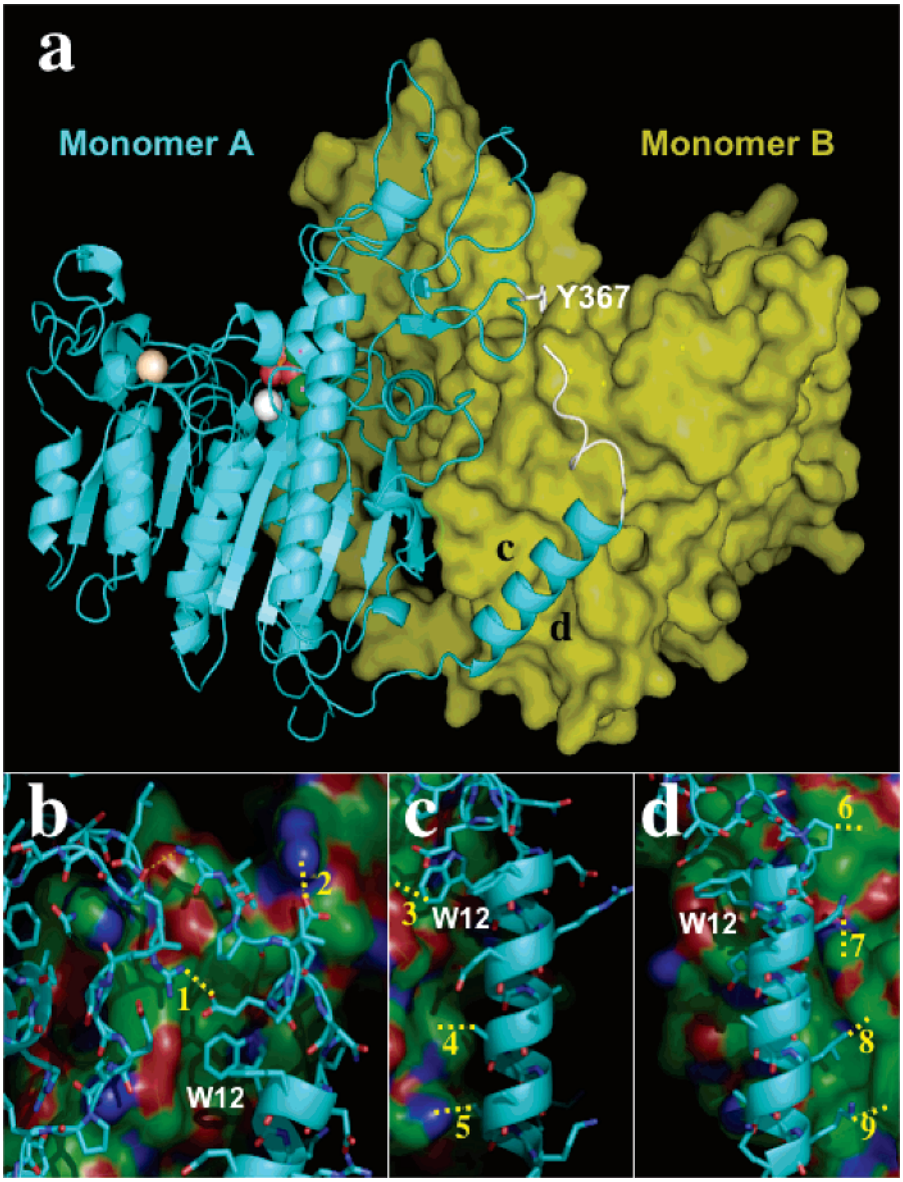

FIGURE 1: N-Terminal PLAP aa residue positioning and interactions. (a) General representation of the PLAP dimer structure. The nine non-α-helical aa residues of monomer A (A) are colored white against the background of monomer B (B). The proximity of these residues to the Y367-harboring loop of A (white) is evidenced. Active site residues PO_4^{3-} (orange), Zn (green), Mg (white), and Ca (wheat) are shown in monomer A. The 16 aa of the N-terminal α-helix of monomer A (between "c" and "d") extend prominently on monomer B. (b) Detailed interactions between N-terminal aa residues of monomer A and the Y367-harboring loop of monomer A and distances between potentially interacting residues: (1) Glu6 (A) and Arg370 (A), 2.86 Å; and (2) Glu7 (A) and Arg117 (B), 2.56 Å. (c and d) Detailed interactions between terminal α-helical residues of monomer A and backbone residues of monomer B, viewed from position c or d, and distances between potentially interacting residues: (3) Trp12 (A) and Lys104 (B), 3.73 Å; (4) Ala19 (A) and Phe457 (B), 3.79 Å; (5) Ala23 (A) and His450 (B), 3.46 Å; (6) Pro9 (A) and Val129 (B), 3.94 Å; (7) Asn13 (A) and His460 (B), 3.2 Å; (8) Leu20 (A) and Tyr471 (B), 3.86 Å; and (9) Lys24 (A) and Phe467 (B), 3.9 Å. Stabilizing bonds are shown as dashed yellow lines, against a background of monomer B. W12 is specified as an internal reference.

(monomer B), separated by 2.56 Å (nr 2). The subsequent 16 aa residues form an α-helix (Figure 1a) and interact with monomer B at several contact points, shown in detail in panels c and d of Figure 1, representing the left and right views of the α-helix as indicated in Figure 1a by the letters "c" and "d", respectively. These figures reveal potential interactions between Pro9 and Val129 (nr 6, 3.94 Å), Trp12 and Lys104 (nr 3, 3.73 Å), Asn13 and His460 (nr 7, 3.2 Å), Ala19 and Phe457 (nr 4, 3.79 Å), Leu20 and Tyr471 (nr 8, 3.86 Å), Ala23 and His450 (nr 5, 3.46 Å), and Lys24 and Phe467 (nr 9, 3.9 Å).

Catalysis in PLAP and TNAP Compared to the General Model of E. coli AP Function. Table 2 shows that the relative PLAP and TNAP activities at pH 9.8 increase approximately 150- and 50-fold, when diethanolamine is progressively added to the buffer, up to 1 M, validating the importance of transphosphorylation in PLAP and TNAP catalysis. Likewise, Table 2 shows a comparable 2.5-fold decrease in the first-order rate constant of the reaction for PLAP and TNAP, with the concentration of sucrose, i.e., when measured in 1 M DEA buffer (pH 9.8) at saturating pNPP concentrations. This is compatible with rate-limiting product dissociation, causing a decrease in k_{cat} when the viscosity increases in the presence of sucrose, as reported for *E. coli* AP at pH 8.0 (*23*). Also, in 1 M Tris-HCl (pH 7.5), increasing concentrations of sucrose weaken the apparent k_{cat} ~2-fold, which is similarly

Table 3: Kinetic Parameters of PLAP, TNAP, and Their Mutants[a]

enzyme	K_m (mM)	k_{cat} (s^{-1})	k_{cat}/K_m ($s^{-1}\ \mu M^{-1}$)
Placental Alkaline Phosphatase (PLAP)			
PLAP−FLAG	0.56 ± 0.1	460 ± 1.5	0.82
PLAP−FLAG (pH 7.5)	0.047 ± 0.0017	11.3 ± 0.3	0.24
[Δ1]PLAP	0.66 ± 0.12	383 ± 74	0.58
(1)PLAP	0.59 ± 0.2	284 ± 15	0.48
[Δ3]PLAP	0.29 ± 0.03	80.9 ± 4.8	0.28
[Δ5]PLAP	0.22 ± 0.03	226 ± 14	1
[Δ7]PLAP	0.3 ± 0.03	118 ± 1.4	0.39
[Δ9]PLAP	0.53 ± 0.06	56.9 ± 3.58	0.11
[Δ9]PLAP (pH 7.5)	0.055 ± 0.0025	2.76 ± 1.5	0.05
[Δ25]PLAP	NA[b]	0	NA[b]
[E7K]PLAP	0.31 ± 0.05	387 ± 34	1.25
[R370A]PLAP	0.51 ± 0.15	199 ± 32	0.39
Tissue-Nonspecific Alkaline Phosphatase (TNAP)			
TNAP−FLAG	0.25 ± 0.02	1102 ± 50	4.5
TNAP−FLAG (pH 7.5)	0.02325 ± 0.0003	22.5 ± 0.9	0.97
[Δ1]TNAP	0.38 ± 0.05	647 ± 55	1.7
(1)TNAP	0.19 ± 0.02	980 ± 58	5.2
[Δ3]TNAP	0.36 ± 0.06	678 ± 22	1.9
[Δ5]TNAP	0.3 ± 0.03	86.4 ± 2.6	0.28
[Δ5]TNAP (pH 7.5)	0.019 ± 0.0002	0.86 ± 0.1	0.045
[Δ9]TNAP	NA[b]	0	NA[b]
[Δ25]TNAP	NA[b]	0	NA[b]
[K7E]TNAP	0.22 ± 0.01	1030 ± 70	4.7
[Y371A]TNAP	0.76 ± 0.11	1717 ± 322	2.3
[R374A]TNAP	1.3 ± 1.6	18.6 ± 4.6	0.01

[a] Due to the low K_i for phosphate, significant inhibition occurs during reactions measured under standard Michaelis−Menten conditions (*24*), using pNPP as a substrate; the kinetic constants are therefore not absolute but allow a relative kinetic comparison among PLAP, TNAP, and their mutants. [b] Not applicable.

compatible with rate-limiting diffusional separation of Tris phosphate from the enzyme at this pH, when measured in the presence of 1 M Tris. In contrast, in the absence of Tris, in 0.04 M Mops (pH 8.0), sucrose has little effect on PLAP and TNAP catalysis (Table 2). Since the rate-limiting hydrolysis of the *E. coli* AP phosphoenzyme intermediate at pH 6 is independent of the viscosity in aqueous sucrose solutions (*23*), these findings imply that, in the absence of transphosphorylation, hydrolysis of the PLAP and TNAP phosphoenzyme intermediate is largely rate-determining, even at pH 8. Finally, similar measurements in 0.04 M Mes buffer (pH 6) confirm the total lack of sucrose on PLAP and TNAP catalysis, compatible with a reaction scheme in which the faint hydrolysis of the phosphoenzyme intermediate is the rate-limiting step at pH 6. However, compared to the first-order rate of PLAP in 1 M DEA buffer (pH 9.8), the relative activity of PLAP is ~35-fold weaker in 1 M Tris-HCl (pH 7.5), 250-fold weaker in 0.04 M Mops (pH 8), and 1500-fold weaker in 0.04 M Mes (pH 6) (Table 2). Likewise, the relative activity of TNAP is ~75-fold weaker in 1 M Tris-HCl (pH 7.5), 600-fold weaker in 0.04 M Mops (pH 8), and 1800-fold weaker in 0.04 M Mes (pH 6) (Table 2). These findings therefore illustrate that, in the absence of transphosphorylation, PLAP and TNAP are poor enzymes, when measured at pH 6 and even at pH 8.

N-Terminal aa Deletions Progressively Affect Catalysis. Analyses of catalytic rate constants for PLAP, TNAP, and their deletion mutants are presented in Table 3, using the known k_{cat} value for PLAP (460 s^{-1}) as a reference. The progressive deletion of the first nine N-terminal aa residues in PLAP caused some fluctuations in the observed catalytic rate constants, measured at pH 9.8, resulting in a considerable decrease in k_{cat} for [Δ9]PLAP (Table 3). Surprisingly the decrease in k_{cat} was not accompanied by a corresponding decrease in K_m. The entire deletion of 25 N-terminal aa residues, including the α-helix, abrogated enzyme activity at pH 9.8, i.e., eliminating catalysis in [Δ25]PLAP. Analysis at pH 7.5 confirmed this conclusion. At this pH, catalysis for PLAP occurs with considerably reduced k_{cat} and K_m values, and with a slightly reduced catalytic efficiency (Table 3). The deletion of the nine N-terminal aa residues did not have an effect on K_m, whereas k_{cat} decreased 4-fold (Table 3). An E7K substitution in PLAP (as found in TNAP), had little impact on catalysis for [E7K]PLAP, at the level of k_{cat} and K_m (Table 3). Mutation of the potential aa ligand for Glu6 in PLAP (Arg370, Figure 1b), likewise, had little impact on catalysis (Table 3). These findings illustrate that amino acid interactions within the first seven N-terminal aa sequence have no impact on the active site of PLAP but that the α-helix plays a crucial role in the PLAP active site function.

Corresponding analyses for TNAP revealed a more prominent impact of N-terminal aa deletion on catalysis. The progressive deletion of N-terminal aa residues in TNAP, likewise, did not affect the K_m for pNPP but strongly reduced k_{cat} (Table 3). Deleting five N-terminal aa residues in [Δ5]TNAP reduced k_{cat} more than 10-fold, at both pH 9.8 and 7.5, without affecting K_m. Further deletion of the next four N-terminal aa residues in [Δ9]TNAP resulted in complete inactivation of the mutant. Correspondingly, [Δ25]TNAP was also inactive. The reciprocal experiment, mentioned above for PLAP, i.e., substituting Lys7 in TNAP for the residue found in PLAP, i.e., K7E, had little effect on catalysis for [K7E]TNAP (Table 3). However, the R374A substitution in TNAP (homologous to R370 in PLAP) resulted in strongly reduced enzyme activity for [R374A]TNAP, at the level of both k_{cat} (50-fold decrease) and K_m (8-fold increase; Table 3, see below).

N-Terminal aa Residue Deletion Does Not Affect AP Active Site Accessibility. Measurements of residual AP activity during inhibition by inorganic phosphate, a competitive inhibitor of APs, revealed that the N-terminal deletion in [Δ9]PLAP had no effect on the IC_{50} for phosphate, when analyzed at pH 9.8, in the presence of 2 mM pNPP (Figure 2a). Likewise, [Δ5]TNAP and TNAP were similarly inhibited by phosphate, indicating that the active site entrance (determined by rate constants k_1 and k_{-1}, like what is shown in the reaction scheme for pNPP), was not affected by the N-terminal deletions that have been investigated. This evidence indicates that k_1 and k_{-1} for substrate positioning in the active site are not modified by the deletion. In all four cases, sigmoidal inhibition curves were found, in agreement with competitive inhibition, but reflecting much stronger inhibition by phosphate of PLAP than of TNAP.

Likewise, inhibition of PLAP and [Δ9]PLAP by uncompetitive inhibitor L-Phe did not differ, and inhibition of TNAP and [Δ5]TNAP by L-homoarginine was identical, when investigated at pH 9.8 (Figure 2). We have confirmed that, also at pH 7.5, PLAP and TNAP were uncompetitively inhibited by L-Phe and L-homoArg, respectively, by constructing double-reciprocal plots of AP activity versus pNPP concentration, for lines constructed at increasing L-Phe (0−20 mM) or L-homoArg concentrations (0−80 mM). These

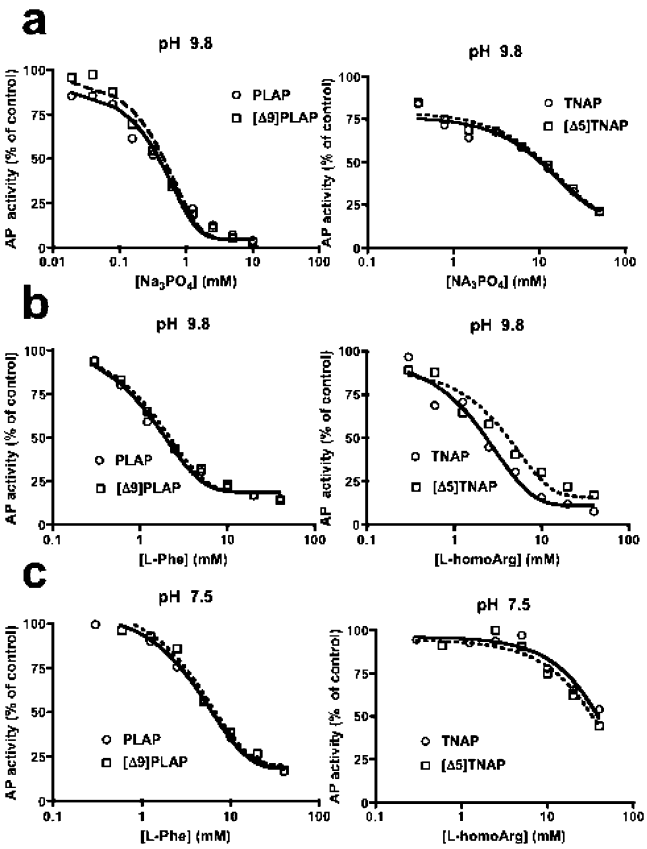

FIGURE 2: Active site inhibition of N-terminal deletion mutants. Dose−response curves for enzyme inhibition of TNAP, PLAP, and their N-terminal deletion mutants [Δ5]TNAP and [Δ9]PLAP by the competitive inhibitor Na_3PO_4 at pH 9.8 (a) and by uncompetitive PLAP inhibitor L-Phe and TNAP inhibitor L-homoArg at pH 9.8 (b) and 7.5 (c). Solid lines (TNAP or PLAP) and dashed lines ([Δ5]TNAP and [Δ9]PLAP) represent fitted inhibition curves.

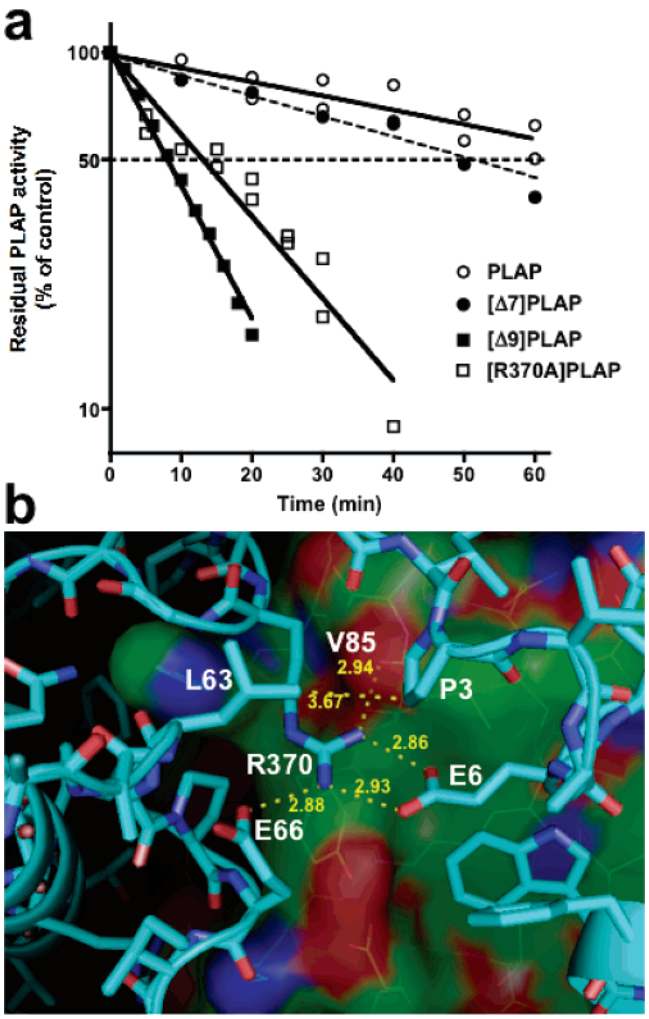

FIGURE 3: Heat inactivation of PLAP and N-terminal deletion and substitution mutants. (a) Residual enzyme activity of wt PLAP (○), [Δ7]PLAP (●) [Δ9]PLAP (■), and [R370A]PLAP (□) as a function of time during an incubation at 65 °C in 1 M DEA buffer, 20 mM $ZnCl_2$, and 1 mM $MgCl_2$ (pH 9.8). (b) Structural interactions in the aa residue microenvironment of Arg370 in PLAP, based on the crystal model in Figure 1.

lines were parallel (not shown), and secondary replots of their ordinate intercepts were linear, yielding a K_i of 7.3 mM for the L-Phe inhibition of PLAP and a K_i of 60 mM for the L-homoArg inhibition of TNAP, values in agreement with the IC_{50} values reported in Figure 2c. The higher IC_{50} values for both inhibitors at pH 7.5 (Figure 2c) are compatible with the uncompetitive mechanism by amino acids that requires the unprotonated amino function of the compounds for inhibition (*5*). These experiments suggested that in the expression for K_i either the k_3/k_2 ratio was not modified during inhibition of the mutants by L-Phe and L-homoArg or, alternatively, $k_3 \ll k_2$, in which case $K_i = K_{EPI}$, for inhibition by these amino acids (*5*).

Heat Inactivation of PLAP and Its Mutants. Figure 3 shows residual AP activity for PLAP and some of its mutants. In agreement with its resistance to high temperatures, PLAP was only mildly inactivated over an interval of 1 h at 65 °C. Deletion of up to the first seven N-terminal residues had little impact on the heat stability of the resulting mutants, shown for [Δ7]PLAP (Figure 3a). However, the additional deletion of two amino acids in [Δ9]PLAP dramatically affected enzyme stability, as assessed via catalytic measurements with pNPP, the monophasic inactivation profile being characterized by a half-life of ∼10 min. Surprisingly, [R370A]PLAP was poorly resistant to heat inactivation, with a half-life of ∼15 min, i.e., comparably unstable as [Δ9]PLAP. These findings illustrate that, despite considerable residual AP activity in [Δ9]PLAP and [R370A]PLAP at room temperature, the resulting mutants were structurally destabilized. More detailed inspection of the microenvironment of Arg370 in the PLAP structure (Figure 3b) revealed that, in addition to Arg370-mediated interactions between the Y367 harboring loop and the N-terminus via Glu6, this residue also interacted with the loop harboring Glu66, as well as with the backbone of the second monomer. In addition, Arg370 is located beneath Leu63, potentially interacting with Pro3, and is therefore relevant in the cross-talk between the N-terminus of PLAP and both loops adjacent to the N-terminus (Figure 1a).

Conformational Analysis of TNAP and Its Deletion Mutants. Since our mutagenesis strategy affected the catalysis of TNAP even more than that of PLAP, the impact of mutagenesis on the structure of TNAP was analyzed in more detail, using a panel of anti-TNAP monoclonal antibodies (*21*, *22*). To exclude antibody recognition sites in the N-terminal aa residues of TNAP as part of the epitope recognized by the antibody panel, first the binding of each antibody to TNAP was investigated in the presence of N-terminal peptides LVPEKEKDP and LVPEKEKDPKY-

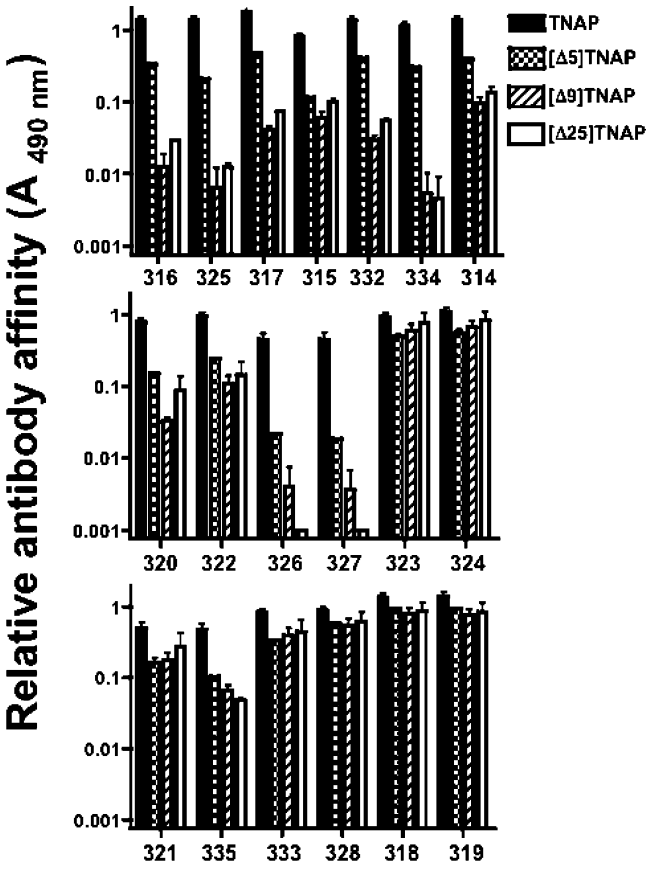

FIGURE 4: Conformational analysis of TNAP and its N-terminal deletion mutants. Structural impact of progressive deletion of N-terminal residues on the affinity for a reference panel of anti-TNAP antibodies (ISOBM TD9 Workshop), coated onto microtiter plates; bound TNAP (mutant) was detected via an ELISA, using anti-FLAG antibody M2 and expressed as *A*(490 nm) for native TNAP, [Δ5]TNAP, [Δ9]TNAP, and [Δ25]TNAP, as indicated. Values are means ± SD of two to four replicates; note the logarithmic scale (antibody division as follows: domain A, 316, 325, 317, 315, and 332; domain B, 334 and 314; domain C, 320, 322, 326, 327, 323, 324, 321, and 335; and domain D, 333, 328, 318, and 319).

WRDQ. None of these peptides interfered with binding of TNAP to microtiter plate-coated antibodies, up to 200 mM peptide (not shown), validating the antibodies as structural probes for monitoring conformational changes in TNAP and its deletion mutants. Figure 4 shows that deletion of five aa residues in [Δ5]TNAP results in weakened recognition by a large number of monoclonal antibodies, arranged according to their identified epitope domains (*21*), whereas the recognition by others, primarily reactive with C-terminal epitopes, is only minimally affected. Additional deletion of four aa residues further reduced the affinity for the first set of antibodies in [Δ9]TNAP, with some antibodies (316, 325, 326, 327, and 334) hardly recognizing [Δ9]TNAP at all. Further deletion of the α-helix affected recognition only minimally in [Δ25]TNAP (Figure 4). These findings illustrate that deletion of five aa residues suffices in affecting the conformation of TNAP and that the additional elimination of four aa residues suffices in eliminating the α-helix-dependent conformational stabilization and catalytic site integrity.

The same analysis for [Y371A]TNAP and [R374A]TNAP (Figure 5) shows that substitution of Tyr371, homologous to Tyr367 in PLAP, does not produce structural destabilization at room temperature in [Y371A]TNAP, as detected by the antibody panel. This finding contrasts sharply with the substitution of Arg374, which results in a strong structural destabilization, as detected by half the number of antibodies in the panel, providing an explanation for the pronounced loss of enzymatic activity in [R374A]TNAP, which is absent in [Y371A]TNAP. Additional heat inactivation studies confirmed that the weak residual enzyme activity of [R374A]TNAP is heat inactivated at 56 °C within 1 min, i.e., much faster than TNAP (Figure 6a). It is also inactivated considerably faster than [Y371A]TNAP, itself being several-fold less heat-stable than TNAP (Figure 6a). The latter finding complies with the reduced heat stability, reported for active site mutant [Y367A]PLAP, compared to that of PLAP (*12*), despite the preserved three-dimensional structural integrity of [Y371A]TNAP at room temperature (Figure 5).

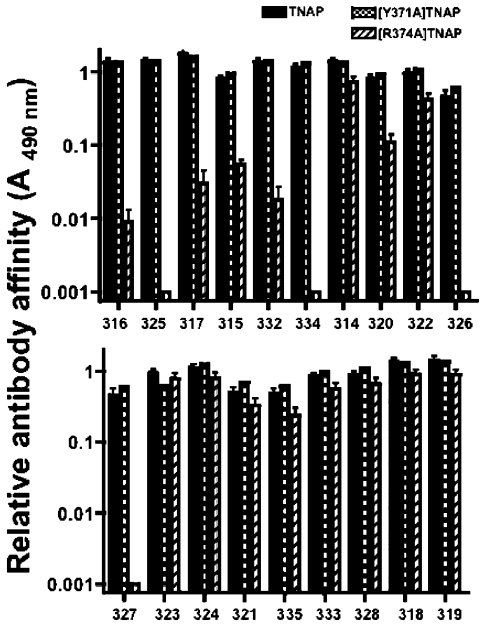

FIGURE 5: Conformational analysis of TNAP and its substitution mutants. Structural impact of mutations in [Y371A]TNAP and [R374A]TNAP on the affinity for a reference panel of anti-TNAP antibodies (ISOBM TD9 Workshop), coated onto microtiter plates; bound TNAP (mutant) was detected, as in Figure 4 for native TNAP, [Y371A]TNAP, and [R374A]TNAP as indicated. Values are means ± SD of two to four replicates; note the logarithmic scale (antibody division as in Figure 4).

DISCUSSION

Many amino acids contribute to the active site integrity in mammalian APs, ranging from residues coordinating the metal ions necessary for substrate positioning and catalysis (*9*, *12*) to residues controlling the orientation of coordinating ligands (*5*, *13*). In addition, a large number of TNAP mutations have been found in patients diagnosed with the genetic disease hypophosphatasia (*18*). These substitutions often cluster at crucial structurally and functionally relevant domains of the enzyme, affect the enzyme's catalytic potential, and cause defective in vivo function for TNAP (*18*, *26*), in turn resulting in various degrees of impaired skeletal mineralization (*27*). Identification of several hypophosphatasia mutations at the N-terminus of TNAP suggested a critical role for the N-terminal arm in the control of TNAP activity. The N-terminus of one monomer embraces the other monomer, but whether this interaction controls the folding,

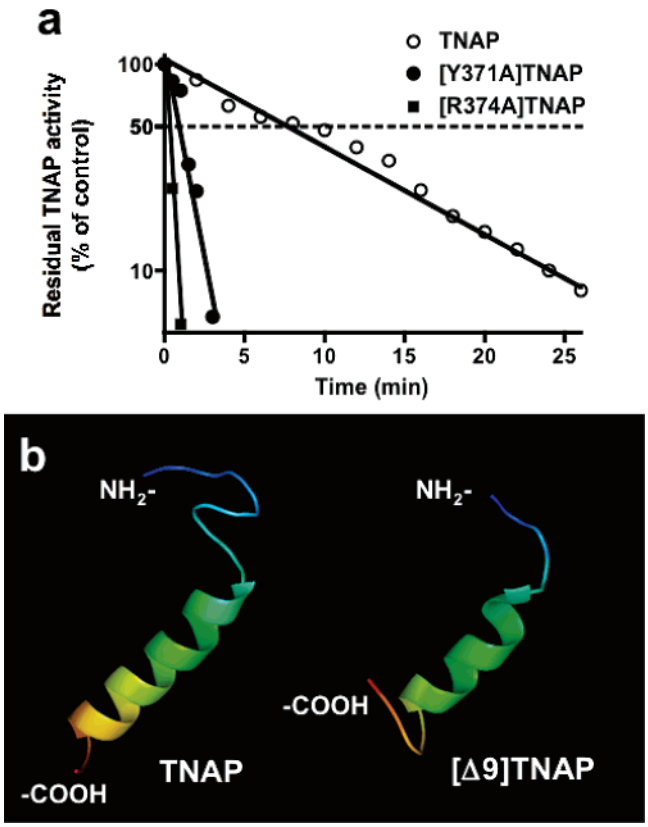

FIGURE 6: Heat inactivation and α-helix propensity of TNAP and substitution mutants. (a) Residual enzyme activity of wt TNAP (○), [Y371A]TNAP (●), and [R374A]TNAP (■) as a function of time during an incubation at 56 °C in 1 M DEA buffer, 20 mM $ZnCl_2$, and 1 mM $MgCl_2$ (pH 9.8). (b) Predicted solution three-dimensional folding of the N-terminal TNAP peptide comprising aa residues 1−25 (TNAP) and 10−25 ([Δ9]TNAP), upon deletion of the N-terminal aa residues 1−9 (NH_2- and -COOH denote the N- and C-terminal ends of the peptides, respectively).

stability, or catalytic function of the enzyme has been unclear. In view of the existence of catalytically relevant hypophosphatasia mutations mapping to the N-terminus of TNAP and in view of our previous work that had shown that single- and multiple-amino acid substitutions at distant locations can influence both the three-dimensional structure of AP dimers as well as its function (*4*, *6*, *28*), we have investigated the function of the N-terminal arm in the control of AP stability. Using the PLAP crystal structure as a paradigm, mutagenesis studies were performed in parallel on PLAP and TNAP, as the latter has only been described by a homology model. In addition, by focusing on individual interactions between N-terminal aa residues and neighboring aa loops, we have identified a critical role for the microenvironment of Arg370 in PLAP and even more so for that of Arg374 in TNAP in the structural control of AP function. To correctly interpret PLAP and TNAP mutations in terms of their functional implications, we also validated the degree to which PLAP and TNAP catalysis complies with the known model of *E. coli* AP enzyme function. At alkaline pH and in the presence of transphosphorylating alcohols, we could confirm that both PLAP and TNAP activity fit the general model, predictive of rate-limiting product release under these conditions.

The existence of potential interactions between amino acids in the N-terminal stretch of nine aa residues and secondary residues in the same and the second monomer as well as several interactions between the next 16 α-helical aa residues and the second monomer backbone were suggested by the PLAP crystal model (*9*). Therefore, a double strategy was used in our studies: progressive deletion of the first amino acids and single-point mutations to investigate contributions to stability, three-dimensional structure, and enzyme function of TNAP and PLAP. Our analysis revealed that deletion of up to seven amino acid residues in PLAP had little impact on catalysis and enzyme stability but that deletion of nine aa affected the catalytic efficiency of the enzyme, due to a decrease in k_{cat}, but not of K_m. Deletion of nine (but not seven or fewer) aa residues was also accompanied by a considerable loss of enzyme stability, as measured via heat inactivation studies. The additional deletion of the α-helix abrogated enzyme activity, reflecting the loss of major structural stabilization by α-helical residues, strongly affecting the AP active site. Since, despite absent Glu6−Arg370 interactions, [Δ7]PLAP exhibited normal stability and catalysis, these findings imply that the structural destabilization of [Δ9]PLAP did not result from elimination of N-terminal aa residues directly involved in structure stabilization but rather suggested that the propensity to form an α-helix in the next 16 aa residues was affected in [Δ9]PLAP, hence destroying its stabilizing interactions, a conclusion supported by the decrease and lack of activity in [Δ9]PLAP and [Δ25]PLAP, respectively. Likewise, interactions between Glu7 and Arg117 in PLAP contributed little, if at all, to enzyme function; a swapping strategy in which Lys7 in TNAP was mutated to Glu7 in PLAP had no effect on catalysis. Yet, although Glu6−Arg370 interactions in PLAP did not contribute to enzyme stability in [Δ7]PLAP, and the R370A mutation affected catalysis only mildly in [R370A]PLAP, Arg370 plays a critical role in stabilizing the three-dimensional structure of PLAP. This residue is located in a microenvironment close to the active site, centrally between the N-terminus and two-aa loops, one of which harbors Y367, an active site determinant (*12*).

Deletion of five aa in TNAP clearly affected AP catalysis in [Δ5]TNAP, in a manner similar to that seen in [Δ9]PLAP, i.e., with a conserved K_m and a reduced k_{cat}. The further elimination of four aa in [Δ9]TNAP abrogated AP catalysis altogether. Structural analysis of this phenomenon, using a panel of epitope-mapped anti-TNAP monoclonal antibodies recognizing epitopes over the entire TNAP structure, confirmed that also in the case of TNAP, the loss of AP catalysis did not result from elimination of critical residues from positions 1−9, but that the progressive deletion of this stretch in [Δ5]TNAP and [Δ9]TNAP affected the role of the α-helix in controlling the three-dimensional structure of TNAP. These findings are supported by the similar reactivity pattern with the antibody panel for [Δ9]TNAP and [Δ25]TNAP, illustrating that the additional deletion of 16 aa residues in [Δ25]TNAP no longer affects the dysfunctional folding observed for [Δ9]TNAP. Hence, the structural deficit in [Δ9]TNAP is comparable to that in [Δ25]TNAP and is larger than that in [Δ9]PLAP, explaining why [Δ9]TNAP is inactive, as opposed to [Δ9]PLAP, which is structurally unstable but still active. The computed α-propensity to form an α-helix supports these conclusions. Figure 6b shows the computed folding for intact TNAP peptide 1−25 and for deleted TNAP peptide 10−25, as present in [Δ9]TNAP, revealing a shorter α-helix.

In view of the structural role of Arg370 in PLAP, it is not surprising that catalysis is more seriously hampered in [R374A]TNAP than in [R370A]PLAP, findings confirming that also in TNAP, this highly conserved residue critically coordinates the cross-talk between several aa loops, adjacent to the active site. This interpretation was confirmed by heat inactivation studies of [R374A]TNAP, and the amazing structural role of Arg374 was also evidenced from the reactivity profile of [R374A]TNAP with the antibody panel, dramatically affected, as measured with many antibodies to the same degree as in [Δ9]TNAP and [Δ25]TNAP. Even though Tyr371 is only three aa residues upstream of R374 and closer to the TNAP active site, its mutagenesis did not affect antibody recognition, further documenting the specific structural role of Arg374 in TNAP.

Despite the decrease in the k_{cat} values of [Δ9]PLAP and [Δ5]TNAP for pNPP, activity measurements in the presence of competitive and uncompetitive inhibitors revealed that PLAP and [Δ9]PLAP, and TNAP and [Δ5]TNAP, were identically inhibited. These findings not only confirmed the preserved active site accessibility in the mutants, as observed during competitive inhibition studies with inorganic phosphate, but also helped us to understand the kinetic consequences of the structural changes introduced into [Δ9]PLAP and [Δ5]TNAP. The phosphate inhibition data confirmed that k_1 and k_{-1} are not affected by these N-terminal deletions. Since the k_{cat}/K_m ratio, apart from k_1 and k_{-1}, depends on only k_2, these data imply that N-terminal aa residue deletions reduce the rate of covalent phospho-complex formation, i.e., k_2; this explains why k_{cat} decreases. Since the expression for k_{cat} and K_m contains a k_2/k_3 term and K_m is not affected by the N-terminal aa deletions, it follows that either $k_2 \ll k_3$ or k_2/k_3 is not affected, implying that the rate of phospho-complex hydrolysis/transphosphorylation (k_3) is reduced, in a manner comparable to that of k_2. The uncompetitive inhibition data confirm that the second option is correct; the expression for K_i contains a k_3/k_2 term, which is identical for deletion mutants and wt enzymes. In view of a modified k_2 in the mutants, these findings would require that $k_3 \ll k_2$, which contradicts the assumption, made above, that $k_2 \ll k_3$. Therefore, the appropriate N-terminal deletions in TNAP and PLAP affect folding of the N-terminal α-helix, which in turn is responsible for structural destabilization, is transferred to the active site, and results in a reduced catalytic efficacy, due to both decelerated phospho-complex formation and subsequent phosphoserine hydrolysis (and transphosphorylation, when measured in diethanolamine at pH 9.8).

In conclusion, this work has shown that the α-helix of the N-terminal arm of one AP monomer that embraces the second monomer is a structural requirement for the active sites to efficiently execute intramolecular transitions during enzyme catalysis in PLAP, but especially in TNAP. Mutations in this arm, deletion of N-terminal aa residues, and mutation of the critical adjacent interacting residue, Arg370 in PLAP or Arg374 in TNAP, result in a loss of enzyme stability and function.

REFERENCES

1. McComb, R. B., Bowers, G. N., Jr., and Posen, S. (1979) *Alkaline phosphatase*, Plenum, New York.
2. Millán, J. L. (2006) *Mammalian alkaline phosphatases. From biology to applications in medicine and biotechnology*, pp 1−322, Wiley-VCH Verlag GmbH & Co., Weinheim, Germany.
3. Hummer, C., and Millan, J. L. (1991) Gly429 is the major determinant of uncompetitive inhibition of human germ cell alkaline phosphatase by L-leucine, *Biochem. J. 274* (Part 1), 91−5.
4. Hoylaerts, M. F., and Millan, J. L. (1991) Site-directed mutagenesis and epitope-mapped monoclonal antibodies define a catalytically important conformational difference between human placental and germ cell alkaline phosphatase, *Eur. J. Biochem. 202*, 605−16.
5. Hoylaerts, M. F., Manes, T., and Millan, J. L. (1992) Molecular mechanism of uncompetitive inhibition of human placental and germ-cell alkaline phosphatase, *Biochem. J. 286* (Part 1), 23−30.
6. Bossi, M., Hoylaerts, M. F., and Millan, J. L. (1993) Modifications in a flexible surface loop modulate the isozyme-specific properties of mammalian alkaline phosphatases, *J. Biol. Chem. 268*, 25409−16.
7. Hoylaerts, M. F., Manes, T., and Millan, J. L. (1997) Mammalian alkaline phosphatases are allosteric enzymes, *J. Biol. Chem. 272*, 22781−7.
8. Wu, L. N., Genge, B. R., Lloyd, G. C., and Wuthier, R. E. (1991) Collagen-binding proteins in collagenase-released matrix vesicles from cartilage. Interaction between matrix vesicle proteins and different types of collagen, *J. Biol. Chem. 266*, 1195−203.
9. Le Du, M. H., Stigbrand, T., Taussig, M. J., Menez, A., and Stura, E. A. (2001) Crystal structure of alkaline phosphatase from human placenta at 1.8 Å resolution. Implication for a substrate specificity, *J. Biol. Chem. 276*, 9158−65.
10. Le Du, M. H., and Millan, J. L. (2002) Structural evidence of functional divergence in human alkaline phosphatases, *J. Biol. Chem. 277*, 49808−14.
11. Llinas, P., Stura, E. A., Menez, A., Kiss, Z., Stigbrand, T., Millan, J. L., and Le Du, M. H. (2005) Structural studies of human placental alkaline phosphatase in complex with functional ligands, *J. Mol. Biol. 350*, 441−51.
12. Kozlenkov, A., Manes, T., Hoylaerts, M. F., and Millan, J. L. (2002) Function assignment to conserved residues in mammalian alkaline phosphatases, *J. Biol. Chem. 277*, 22992−9.
13. Kozlenkov, A., Le Du, M. H., Cuniasse, P., Ny, T., Hoylaerts, M. F., and Millan, J. L. (2004) Residues determining the binding specificity of uncompetitive inhibitors to tissue-nonspecific alkaline phosphatase, *J. Bone Miner. Res. 19*, 1862−72.
14. Hessle, L., Johnson, K. A., Anderson, H. C., Narisawa, S., Sali, A., Goding, J. W., et al. (2002) Tissue-nonspecific alkaline phosphatase and plasma cell membrane glycoprotein-1 are central antagonistic regulators of bone mineralization, *Proc. Natl. Acad. Sci. U.S.A. 99*, 9445−9.
15. Harmey, D., Hessle, L., Narisawa, S., Johnson, K. A., Terkeltaub, R., and Millan, J. L. (2004) Concerted regulation of inorganic pyrophosphate and osteopontin by akp2, enpp1, and ank: An integrated model of the pathogenesis of mineralization disorders, *Am. J. Pathol. 164*, 1199−209.
16. Henthorn, P. S., Raducha, M., Fedde, K. N., Lafferty, M. A., and Whyte, M. P. (1992) Different missense mutations at the tissue-nonspecific alkaline phosphatase gene locus in autosomal recessively inherited forms of mild and severe hypophosphatasia, *Proc. Natl. Acad. Sci. U.S.A. 89*, 9924−8.
17. Zurutuza, L., Muller, F., Gibrat, J. F., Taillandier, A., Simon-Bouy, B., Serre, J. L., et al. (1999) Correlations of genotype and phenotype in hypophosphatasia, *Hum. Mol. Genet. 8*, 1039−46.
18. Mornet, E., Stura, E., Lia-Baldini, A. S., Stigbrand, T., Menez, A., and Le Du, M. H. (2001) Structural evidence for a functional role of human tissue nonspecific alkaline phosphatase in bone mineralization, *J. Biol. Chem. 276*, 31171−8.
19. Taillandier, A., Lia-Baldini, A. S., Mouchard, M., Robin, B., Muller, F., Simon-Bouy, B., et al. (2001) Twelve novel mutations in the tissue-nonspecific alkaline phosphatase gene (ALPL) in patients with various forms of hypophosphatasia, *Hum. Mutat. 18*, 83−4.
20. Henthorn, P. S., and Whyte, M. P. (1992) Missense mutations of the tissue-nonspecific alkaline phosphatase gene in hypophosphatasia, *Clin. Chem. 38*, 2501−5.
21. Magnusson, P., Arlestig, L., Paus, E., Di Mauro, S., Testa, M. P., Stigbrand, T., et al. (2002) Monoclonal antibodies against tissue-nonspecific alkaline phosphatase. Report of the ISOBM TD9 workshop, *Tumor Biol. 23*, 228−48.

22. Narisawa, S., Harmey, D., Magnusson, P., and Millan, J. L. (2005) Conserved epitopes in human and mouse tissue-nonspecific alkaline phosphatase. Second report of the ISOBM TD-9 workshop, *Tumor Biol. 26*, 113−20.
23. Simopoulos, T. T., and Jencks, W. P. (1994) Alkaline phosphatase is an almost perfect enzyme, *Biochemistry 33*, 10375−80.
24. O'Brien, P. J., and Herschlag, D. (2002) Alkaline phosphatase revisited: Hydrolysis of alkyl phosphates, *Biochemistry 41*, 3207−25.
25. Trentham, D. R., and Gutfreund, H. (1968) The kinetics of the reaction of nitrophenyl phosphates with alkaline phosphatase from *Escherichia coli*, *Biochem. J. 106*, 455−60.
26. Di Mauro, S., Manes, T., Hessle, L., Kozlenkov, A., Pizauro, J. M., Hoylaerts, M. F., et al. (2002) Kinetic characterization of hypophosphatasia mutations with physiological substrates, *J. Bone Miner. Res. 17*, 1383−91.
27. Whyte, M. P. (1994) Hypophosphatasia and the role of alkaline phosphatase in skeletal mineralization, *Endocr. Rev. 15*, 439−61.
28. Hoylaerts, M. F., Manes, T., and Millan, J. L. (1992) Allelic amino acid substitutions affect the conformation and immunoreactivity of germ-cell alkaline phosphatase phenotypes, *Clin. Chem. 38*, 2493−500.

BI052471+